



Cite this: *Chem. Commun.*, 2024, 60, 13051

Received 16th September 2024,  
Accepted 10th October 2024

DOI: 10.1039/d4cc04798b

rsc.li/chemcomm

# Reversible CO<sub>2</sub> insertion into the silicon–nitrogen σ-bond of an N-heterocyclic iminosilane†

Jingyan Wang, Gi Byoung Hwang, Caroline E. Knapp and Daniel W. N. Wilson \*

**The reversible insertion of carbon dioxide into the silicon–nitrogen bond of an N-heterocyclic iminosilane is reported. Solution-phase thermodynamic investigations indicate that this process is thermoneutral and reversible, whereas in the solid-phase CO<sub>2</sub> can be stored for extended periods and is only released upon heating to 133 °C.**

The rising atmospheric concentration of the greenhouse gas carbon dioxide (CO<sub>2</sub>) is an urgent pressing global concern. New technologies for the capture, storage, or valorization of CO<sub>2</sub> from flu gas or directly from the air help mitigate the detrimental effects of CO<sub>2</sub> atmospheric accumulation.<sup>1,2</sup> The ability to reversibly bind and store CO<sub>2</sub> through the formation of weak, easily breakable chemical bonds creates energetically efficient carbon fixation pathways.<sup>3</sup> Additionally, such potential energy landscapes are ideal for the development of catalysts which can convert CO<sub>2</sub> into industrially useful feedstocks.<sup>4</sup> Technologies based on earth abundant elements would provide a sustainable route to CO<sub>2</sub> utilization.<sup>5</sup> A variety of low-valent transition metal (TM) and p-block Lewis bases can coordinate to the electrophilic carbon of CO<sub>2</sub> to form zwitterionic complexes.<sup>6</sup> Amongst these, nitrogen bases are particularly desirable due to their low cost and ease of synthetic access (Fig. 1A). Amidine- and guanidine-derived superbases bind CO<sub>2</sub> weakly and can catalyse its reduction to a variety of products, including amide and methanol-precursors.<sup>6–10</sup> Recently, compounds featuring the imidazolin-2-imino group (N-heterocyclic imines) have been reported which can capture CO<sub>2</sub> and release it upon heating or photolysis, highlighting their potential use for CO<sub>2</sub> storage.<sup>11,12</sup>

In addition to Lewis acid–base complexes, CO<sub>2</sub> can insert into homo- and hetero-element σ-bonds.<sup>13,14</sup> The best studied systems

in this class feature late TM–E bonds, where E can be a hydride or p-block element (Fig. 1; B. E = H, OR, NR<sub>2</sub>, CR<sub>3</sub>, SiR<sub>3</sub>), in which CO<sub>2</sub> insertion is an elementary step preceding CO<sub>2</sub> valorization.

The insertion of CO<sub>2</sub> into earth abundant and inexpensive p-block element–element bonds would provide an alternative to TMs, however such insertions typically yield thermodynamically stable products which do not easily release CO<sub>2</sub>, and requiring catalytic strategies with large driving forces (*e.g.* high temperatures).<sup>6</sup> Examples of reversible CO<sub>2</sub> activation by p-block complexes include bonds between divalent group 14 elements, Ge<sup>2+</sup>–Ge<sup>2+</sup> and Sn<sup>2+</sup>–Sn<sup>2+</sup>,<sup>15</sup> and select Lewis acid–base adducts (including Sn–P, In–P, N–Al complexes) which can dissociate to capture CO<sub>2</sub>.<sup>16–18</sup> In these cases, high temperatures and reduced pressures are needed to induce loss of CO<sub>2</sub>, rendering them incompatible to thermodynamic study requiring closed systems and limiting the understanding of their mechanisms.

Here, we report the reversible, thermoneutral capture of CO<sub>2</sub> by a N–Si bond. The solution phase thermodynamic parameters for the insertion reaction were determined by variable temperature NMR experiments, and the mechanism was further elucidated



**Fig. 1** (A) Previous examples of nitrogen-bases which coordinate CO<sub>2</sub>. (B) The insertion of CO<sub>2</sub> into transition metal (M)–heteroatom (E) bonds (L = ligand). (C) This work: the reversible insertion of CO<sub>2</sub> into a nitrogen–silicon bond.

Department of Chemistry, University College London, 20 Gordon Street, London, UK. E-mail: dan.wilson@ucl.ac.uk

† Electronic supplementary information (ESI) available: Data for this article, including experimental procedures, computational details, crystallographic data and NMR spectra. The data supporting this article have been included as part of the ESI. Crystallographic data for 1 has been deposited at the CCDC 2384340 (1). For ESI and crystallographic data in CIF or other electronic format see DOI: <https://doi.org/10.1039/d4cc04798b>



using density functional theory calculations. Thermogravimetric analysis indicates that CO<sub>2</sub> can be stored in the solid state up to 133 °C, at which point reformation of the starting material occurs. Contrasting this, dissolution of the solids results in release of CO<sub>2</sub> under ambient conditions, presenting a novel route to molecular CO<sub>2</sub> storage.

N-heterocyclic imines typically bind CO<sub>2</sub> through coordination of the imine nitrogen to the electrophilic CO<sub>2</sub> carbon, forming zwitterionic acid-base adducts.<sup>11,12</sup> The steric and electronic properties of the NHC have been shown to affect the binding energy of the N–CO<sub>2</sub> bond.<sup>11</sup> However, there has been little exploration of how modifying the imine substituent influences reactivity. We hypothesized that modifying the electropositivity, oxophilicity, and/or covalency of the imine substituent would allow for Sigma-bond insertions analogous to those observed in TM–E compounds.<sup>13</sup> Exposure of a benzene solution of **IPrNSiMe<sub>3</sub>**<sup>19</sup> (IPr = 1,3-di(2',6'-diisopropylphenyl)imidazolin-2-ylidene) to CO<sub>2</sub> (1 Bar; Scheme 1) results in the appearance of new resonances in the <sup>1</sup>H NMR spectrum alongside the resonances associated with the starting material (Fig. S2, ESI†). Neither addition of further CO<sub>2</sub> nor heating resulted in complete conversion to the product, and removal of the CO<sub>2</sub> gas from the headspace of the reaction resulted in a loss of intensity of the resonances associated with the product concomitant with an increase in intensity for the **IPrNSiMe<sub>3</sub>** resonances, consistent with a reversible reaction. Performing the reaction in hexane, a low polarity solvent, at –35 °C allowed for the isolation of analytically pure, colourless crystals of **IPrNCO<sub>2</sub>SiMe<sub>3</sub>** (**1**, isolated in 76% yield).

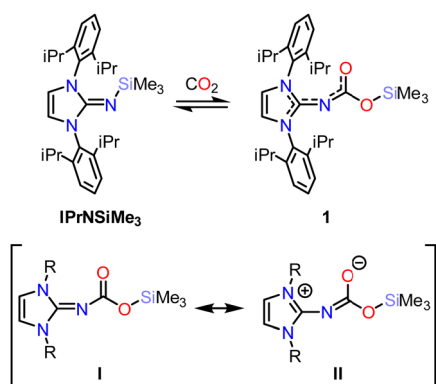
The crystal structure of **1** (Fig. 2; top) revealed CO<sub>2</sub> insertion into the N–Si bond of **IPrNSiMe<sub>3</sub>**, rather than formation of an acid-base adduct as observed in previous studies on alkyl-substituted N-heterocyclic imines.<sup>11,12</sup> The C1–N1 distance is 1.319(2) Å, elongated with respect to the precursor (*cf.* 1.265(3) Å)<sup>19</sup> indicating reduced double bond character with respect to **IPrN–SiMe<sub>3</sub>**. The N1–C2 distance is 1.3434(15) Å, falling within the expected distance for single (1.46 Å)<sup>20</sup> and double bonds (1.27 Å), in line with contribution from both the neutral (Scheme 1; I) and zwitterionic (II) resonance structures of **1**. The C2–O1 and C2–O2 bonds are 1.3636(14) and 1.2272(15) Å, respectively, slightly contracted with respect to the expected distance for single (1.38 Å)



**Fig. 2** Top: Crystal structure of **1**. The thermal ellipsoids are drawn at 50% probability. The diisopropyl and methyl carbon atoms are shown as spheres or arbitrary radius, and most hydrogen atoms are omitted for clarity. Key bond lengths (Å) and angles (°): C1–N1, 1.3187(15); N1–C2, 1.3434(15); C2–O2, 1.2272(15); C2–O1, 1.3636(14); O1–Si1, 1.6712(9). C1–N1–C2, 119.80(10); N1–C2–O1, 110.87(10); O2–C2–N1, 128.96(11); O2–C2–O1, 120.09(11). Bottom: FTIR spectra of **IPrNSiMe<sub>3</sub>** (red) showing strong absorption at 1695 cm<sup>–1</sup> and **1** (blue) showing new absorptions at 1613 and 1558 cm<sup>–1</sup>.

and double (1.24 Å) bonds. Despite significant delocalization throughout the conjugated atoms, which would benefit from planarity to maximise overlap between  $\pi$ -orbitals, the NCO<sub>2</sub>SiMe<sub>3</sub> moiety is twisted out of the NHC plane by 47°. This is likely due to steric hinderance of the diisopropylphenyl groups. Notably, **1** is sensitive to hydrolysis and liberates CO<sub>2</sub> upon exposure to water to yield **IPrNH**.

Fourier-transform infrared (FTIR) analysis performed on crystalline **1** was consistent with complete consumption of **IPrNSiMe<sub>3</sub>**, evidenced by the loss of the diagnostic carbonic C<sub>NHC</sub>=N stretch at 1695 cm<sup>–1</sup> (Fig. 2). New stretches at 1613 and 1558 cm<sup>–1</sup> were present in the spectrum of **1**, which we assign as the C<sub>NHC</sub>=N stretch and the CO<sub>2</sub> asymmetric stretch, respectively, the former is in keeping with the reduction of C<sub>NHC</sub>–N bond order observed in the solid state, and further supports contribution from the zwitterionic resonance structure. Dissolving the crystals of **1** resulted in the reappearance of **IPrNSiMe<sub>3</sub>** in the <sup>1</sup>H NMR spectrum, and leaving the system open to atmosphere or applying vacuum converts the mixture to **IPrNSiMe<sub>3</sub>**, indicating that the two species are in equilibrium. While p-block systems capable of CO<sub>2</sub> capture are known,<sup>21–24</sup> there are few examples of reversible CO<sub>2</sub> capture,<sup>15–17</sup> and fewer still are amenable to mechanistic



**Scheme 1** Top: Equilibrium between **IPrNSiMe<sub>3</sub>** and **1**. Bottom: Neutral (I) and zwitterionic (II) resonance structures of **1** (R = 2,6-diisopropylphenyl).





Fig. 3 Top: Variable temperature  $^1\text{H}$  NMR (500 MHz, toluene- $d_8$ , 298–333 K) studies under 1 bar  $\text{CO}_2$ . Region highlighted blue corresponds to resonances associated with **1**, while red corresponds to **IPrNSiMe<sub>3</sub>**. Bottom: van't Hoff plot of  $\ln(K_{\text{CO}_2})$  vs.  $1/T$ .

study.<sup>25,26</sup> Because of the reversibility of  $\text{CO}_2$  binding under ambient conditions, **IPrNSiMe<sub>3</sub>** presents an ideal platform for such study.

The presence of well-defined and unbroadened  $^1\text{H}$  NMR resonances for **IPrNSiMe<sub>3</sub>** and **1** indicates slow chemical exchange with respect to the NMR timescale (500 MHz). Variable temperature (VT) NMR studies performed on a solution of **IPrNSiMe<sub>3</sub>** under 1 bar of  $\text{CO}_2$  allowed for the determination of thermodynamic parameters for the equilibrium ( $\Delta H^\circ$ ,  $\Delta S^\circ$ , and  $\Delta G^\circ$ ) by linear regression of the van't Hoff plot of  $\ln(K_{\text{CO}_2})$  vs.  $1/T$  (Fig. 3). Giving value of  $\Delta H^\circ = -61 \pm 1 \text{ kJ mol}^{-1}$ ,  $\Delta S^\circ = -194 \pm 4 \text{ J mol}^{-1}$ , and  $\Delta G^\circ = -3.3 \pm 0.1 \text{ kJ mol}^{-1}$ . The reaction is overall slightly endergonic, with a relatively large negative enthalpy, consistent with the formation of new N–C and O–Si bonds, and a negative entropy as expected from a condensation reaction.

Self-exchange rates were extracted from the VT NMR analysis.<sup>27</sup> Due to the slow rate of equilibrium, no line broadening was observed and the rate of exchange between **1** and **IPrNSiMe<sub>3</sub>** was determined from the integration of NMR peaks. We propose the mechanism of interconversion of **1** + **IPrNSiMe<sub>3</sub>**  $\rightleftharpoons$  **IPrNSiMe<sub>3</sub>** + **1** occurs *via* dissociation of  $\text{CO}_2$  from **1**, followed by association of  $\text{CO}_2$  to **IPrNSiMe<sub>3</sub>** (Fig. S7, ESI†), where the rate limiting step is the dissociation of  $\text{CO}_2$  ( $k_{\text{loss}}$ ) (see ESI† Section S4.0). Eyring plots of  $\ln(k_{\text{loss}}/T)$  vs.  $1/T$  (Fig. S8, ESI†) allowed for the determination of activation parameters of  $\text{CO}_2$  loss:  $\Delta H_{\text{loss}}^\ddagger = +32 \pm 0.6 \text{ kJ mol}^{-1}$ ,

$\Delta S_{\text{loss}}^\ddagger = -95 \pm 24 \text{ J mol}^{-1}$  and  $\Delta G_{\text{loss}}^\ddagger = +61 \pm 7 \text{ kJ mol}^{-1}$ . Further, from the relationship  $\Delta G_{\text{loss}}^\ddagger = \Delta G_{\text{bind}}^\ddagger - \Delta G^\circ$ ,  $\Delta G_{\text{bind}}^\ddagger$  can be estimated as  $+64 \pm 7 \text{ kJ mol}^{-1}$ .

Density functional theory (DFT) calculations were performed to gain further insight into the mechanism of  $\text{CO}_2$  binding. A variety of basis sets and functional combinations were screened (see ESI†, 8.0).<sup>28,29</sup> Notably, the thermodynamics of the reaction were highly dependent on the method employed. Pople basis sets resulted in highly exergonic reactions with reverse barriers too large to be reversible at room temperature (e.g. for PBE/6311++g-D3  $\Delta G_{\text{calc}} = -55 \text{ kJ mol}^{-1}$ ,  $\Delta G_{\text{reverse}}^\ddagger = +131 \text{ kcal mol}^{-1}$ ). The method BP86/def2-TZVP-D3 gave forward (+71  $\text{kJ mol}^{-1}$ ) and reverse (+73  $\text{kJ mol}^{-1}$ ) energetic barriers which were slightly overestimated with respect to the experimentally determined barrier (cf.  $+64 \pm 7 \text{ kJ mol}^{-1}$ ) however qualitatively reproduces the reaction energetics (Fig. 4). An energetically reasonable mechanism involves initial coordination of  $\text{CO}_2$  to the imine to form the zwitterionic intermediate (**Int1**). Contrasting previously reported and isolable N-heterocyclic imine- $\text{CO}_2$  adducts, **Int1** is significantly higher in energy than the starting molecules (+68  $\text{kcal mol}^{-1}$ ), possibly due to steric clash between the diisopropylphenyl groups and the  $\text{CO}_2$  moiety.<sup>11</sup> The energetic barrier between **Int1** and **1** is small (12  $\text{kJ mol}^{-1}$ ) and proceeds *via* a 4-membered transition state (**TS2**) in which the silyl group migrates from the nitrogen to the oxygen. The overall reaction, **IPrNSiMe<sub>3</sub>** +  $\text{CO}_2 \rightarrow \textbf{1}$ , is slightly endergonic ( $\Delta G_{\text{calc}} = +11 \text{ kJ mol}^{-1}$ ), contrasting the experimentally determined  $\Delta G^\circ = -3.3 \pm 0.1 \text{ kJ mol}^{-1}$ . The difference between experimental and computational free energy is small and is likely due to errors associated with the methodology employed, which even in the best case can be as much as 8  $\text{kJ mol}^{-1}$ ,<sup>28</sup> and the limitations of DFT in accurately accounting for the entropy associated with solvating gas-phase molecules, in this case  $\text{CO}_2$ .<sup>30</sup>

Reducing the steric bulk at the N-heterocyclic carbene moiety in the calculated models (Dipp  $\rightarrow$  Me; PBE/6311g++/D3) did not impact the qualitative reaction profile, with **Int1**<sup>Me</sup> significantly higher in energy in comparison to reactants and products ( $\Delta G^\ddagger = +44 \text{ kcal mol}^{-1}$ ,  $\Delta G_{\text{calc}} = +6 \text{ kJ mol}^{-1}$ ). This



Fig. 4 Calculated reaction mechanism and potential energy surface (in  $\text{kJ mol}^{-1}$ ) for the conversion of **IPrNSiMe<sub>3</sub>** to **1**. Method: BP86/def2-TZVP-D3 with the application of a continuum solvation model to mimic the effect of benzene solvent.  $R = 2,6$ -diisopropylphenyl.





Fig. 5 Thermogravimetric plot for **1** (solid line), and its first derivative (dashed line). Shaded blue area shows the area integrating as 8.7% of total sample mass.

indicates that the electropositivity and propensity for migration of silane in comparison to carbon substituents facilitates the migration, rather than the reaction being driven by release of steric clash.

Having established the solution-phase behaviour of **1**, we sought to assess if **1** could store and release CO<sub>2</sub> in the solid state. Thermogravimetric analysis on crystalline **1** revealed two features, a sharp decrease at 133 °C followed by a broad feature beginning after 200 °C and centered at 347 °C (Fig. 5). Plotting the first derivative of the curve revealed two separate events, with the area under the first peak integrating as 8.7% of the total sample mass, in agreement with the theoretical mass of CO<sub>2</sub> in the sample (8.5%). FTIR analysis of crystals of **1** heated to 140 °C showed loss of the absorbances associated with the CO<sub>2</sub> stretch and reappearance of the peak at 1695 cm<sup>-1</sup>. Dissolving the resultant solids displayed the diagnostic <sup>1</sup>H NMR resonances associated with **IPrNSiMe<sub>3</sub>**. Therefore, in the solid-state CO<sub>2</sub> is released and **IPrNSiMe<sub>3</sub>** can be reformed. The temperature at which **1** releases CO<sub>2</sub> is higher than those reported for N-heterocyclic imine-CO<sub>2</sub> adducts, which decarboxylate between 30 and 100 °C, depending on the identity of the NHC moiety and its substituents.<sup>11</sup>

In summary, we have demonstrated the capture of CO<sub>2</sub> by an N-heterocyclic iminosilane. In the solution-phase, NMR experiments demonstrate that this reaction is almost thermoneutral and fully reversible, while in the solid-state CO<sub>2</sub> can be stored for extended periods up to 133 °C. Computations indicate that the reversibility of this reaction is due to the oxophilicity of the silane substituent.

D. W. N. W. thanks the Royal Commission for the Exhibition 1851 (RF2023DW) and the Royal Society of Chemistry (R23-4527710839) for funding. We thank Dr Abil Aliev (UCL) for assistance with NMR measurements.

## Data availability

Data for this article, including experimental procedures, computational details, crystallographic data and NMR spectra. The

data supporting this article have been included as part of the ESI.† Crystallographic data for **1** has been deposited at the CCDC under 2384340.

## Conflicts of interest

There are no conflicts to declare.

## Notes and references

- 1 M. Aresta, A. Dibenedetto and A. Angelini, *Chem. Rev.*, 2014, **114**, 1709–1742.
- 2 E. S. Sanz-Pérez, C. R. Murdock, S. A. Didas and C. W. Jones, *Chem. Rev.*, 2016, **116**, 11840–11876.
- 3 L. J. Murphy, K. N. Robertson, R. A. Kemp, H. M. Tuononen and J. A. C. Clyburne, *Chem. Commun.*, 2015, **51**, 3942–3956.
- 4 L. Zhao, H.-Y. Hu, A.-G. Wu, A. O. Terent'ev, L.-N. He and H.-R. Li, *J. CO<sub>2</sub> Util.*, 2024, **82**, 102753.
- 5 K. M. P. Wheelhouse, R. L. Webster and G. L. Beutner, *Org. Process Res. Dev.*, 2023, **27**, 1157–1159.
- 6 P. Sreejyothi and S. K. Mandal, *Chem. Sci.*, 2020, **11**, 10571–10593.
- 7 C. Villiers, J.-P. Dognon, R. Pollet, P. Thuéry and M. Ephritikhine, *Angew. Chem., Int. Ed.*, 2010, **49**, 3465–3468.
- 8 C. Das Neves Gomes, O. Jacquet, C. Villiers, P. Thuéry, M. Ephritikhine and T. Cantat, *Angew. Chem., Int. Ed.*, 2012, **51**, 187–190.
- 9 H. Zhou, W. Chen, J.-H. Liu, W.-Z. Zhang and X.-B. Lu, *Green Chem.*, 2020, **22**, 7832–7838.
- 10 J. K. Mannisto, L. Pavlovic, T. Tiainen, M. Nieger, A. Sahari, K. H. Hopmann and T. Repo, *Catal. Sci. Technol.*, 2021, **11**, 6877–6886.
- 11 L. F. B. Wilm, T. Eder, C. Mück-Lichtenfeld, P. Mehlmann, M. Wünsche, F. Buß and F. Dielmann, *Green Chem.*, 2019, **21**, 640–648.
- 12 L. F. B. Wilm, M. Das, D. Janssen-Müller, C. Mück-Lichtenfeld, F. Glorius and F. Dielmann, *Angew. Chem., Int. Ed.*, 2022, **61**, e202112344.
- 13 N. Hazari and J. E. Heimann, *Inorg. Chem.*, 2017, **56**, 13655–13678.
- 14 A. P. Deziel, M. R. Espinosa, L. Pavlovic, D. J. Charboneau, N. Hazari, K. H. Hopmann and B. Q. Mercado, *Chem. Sci.*, 2022, **13**, 2391–2404.
- 15 A. Caise, L. P. Griffin, C. McManus, A. Heilmann and S. Aldridge, *Angew. Chem., Int. Ed.*, 2022, **61**, e202117496.
- 16 D. A. Dickie, E. N. Coker and R. A. Kemp, *Inorg. Chem.*, 2011, **50**, 11288–11290.
- 17 D. A. Dickie, M. T. Barker, M. A. Land, K. E. Hughes, J. A. C. Clyburne and R. A. Kemp, *Inorg. Chem.*, 2015, **54**, 11121–11126.
- 18 T. W. Yokley, H. Tupkar, N. D. Schley, N. J. DeYonker and T. P. Brewster, *Eur. J. Inorg. Chem.*, 2020, 2958–2967.
- 19 M. Tamm, S. Randoll, E. Herdtweck, N. Kleigrew, G. Kehr, G. Erker and B. Rieger, *Dalton Trans.*, 2006, 459–467.
- 20 P. Pyykkö, *J. Phys. Chem. A*, 2015, **119**, 2326–2337.
- 21 D. Sarkar, L. Groll, D. Munz, F. Hanusch and S. Inoue, *ChemCatChem*, 2022, **14**, e202201048.
- 22 F. Gründler, H. Scholz, M. Herbig, S. Schwarzer, J. Wagler and E. Kroke, *Euro. J. Inorg. Chem.*, 2021, 2211–2224.
- 23 K. Kraushaar, C. Wiltzsch, J. Wagler, U. Böhme, A. Schwarzer, G. Roewer and E. Kroke, *Organometallics*, 2012, **31**, 4779–4785.
- 24 M. Reißmann, A. Schäfer, S. Jung and T. Müller, *Organometallics*, 2013, **32**, 6736–6744.
- 25 C. M. Mömming, E. Otten, G. Kehr, R. Fröhlich, S. Grimme, D. W. Stephan and G. Erker, *Angew. Chem., Int. Ed.*, 2009, **48**, 6643–6646.
- 26 F. Buß, P. Mehlmann, C. Mück-Lichtenfeld, K. Bergander and F. Dielmann, *J. Am. Chem. Soc.*, 2016, **138**, 1840–1843.
- 27 R. C. Cammarota, J. Xie, S. A. Burgess, M. V. Vollmer, K. D. Vogiatzis, J. Ye, J. C. Linehan, A. M. Appel, C. Hoffmann, X. Wang, V. G. Young and C. C. Lu, *Chem. Sci.*, 2019, **10**, 7029–7042.
- 28 M. Bursch, J.-M. Mewes, A. Hansen and S. Grimme, *Angew. Chem., Int. Ed.*, 2022, **61**, e202205735.
- 29 B. A. Shiekh, *ACS Omega*, 2019, **4**, 15435–15443.
- 30 S.-C. Liu, X.-R. Zhu, D.-Y. Liu and D.-C. Fang, *Phys. Chem. Chem. Phys.*, 2023, **25**, 913–931.

